

The May 2024 Storm: dayside magnetopause and cusps in simulated soft X-Rays

J. Ng^{1,2}, L.-J. Chen², B. Burkholder², D. Sibeck², F. S. Porter², K. H. Pham³, V. G. Merkin³, H. Connor², J. W. Bonnell⁴, S. Petrinec⁵, Y. Zou³, B. Alterman², G. Cucho-Padin²

¹Department of Astronomy, University of Maryland, College Park, MD

²NASA Goddard Space Flight Center, Greenbelt, MD

³Applied Physics Laboratory, Johns Hopkins University, Laurel, MD

⁴Space Sciences Laboratory, University of California, Berkeley, CA

⁵Lockheed Martin Advanced Technology Center, Palo Alto, CA, USA

Key Points:

- Reconstructed X-Ray imaging show magnetopause location variations consistent with observations and simulations
- The cusps in X-Ray images expand poleward from nearly parallel to each other as the IMF B_z reverses from southward to northward.
- Intense northern over southern cusp asymmetry is distinguished in X-Ray and understood as due to sunward dipole tilt and the solar wind flow into the cusp.

Corresponding author: Jonathan Ng, jonng@umd.edu

Abstract

The coronal mass ejection (CME) arriving at Earth on May 10, 2024 caused the most intense geomagnetic storm in the last two decades, and resulted in highly unusual magnetopause and cusp dynamics. We simulate soft X-Ray emission due to solar wind charge exchange with exospheric neutrals to image the global dayside dynamics, focusing on the impact of a dense CME current sheet during the storm main phase. The magnetopause moves inward to $\sim 4 R_E$, and at the same time, the two cusps manifest as nearly parallel emission ridges in X-Ray. As the interplanetary magnetic field reverses, the cusp ridges move to higher latitudes for ~ 10 minutes after the reversal. The X-Ray emission can be detected by imagers to be flown on future missions to provide a global picture of the magnetopause and cusps with quantitative determination of their locations.

Plain Language Summary

X-rays are produced when heavy ions in the solar wind and neutral hydrogen in the vicinity of the Earth interact. When captured by imagers, these X-rays are able to provide a view of the global magnetospheric structure. On May 10, 2024, a coronal mass ejection (CME) arriving at Earth caused the most intense geomagnetic storm in the last two decades, pushing the boundary between Earth’s dipole and the interplanetary magnetic field inwards to $\sim 4R_E$. We use simulations to reconstruct how this would have appeared using X-ray diagnostics, which will be used on future missions such as SMILE.

1 Introduction

The May 2024 storm, also known as the Mother’s Day storm or the Gannon storm, is the most intense storm in the last two decades. During the storm, the negative peak of Sym-H reached -518 nT (Tulasi Ram et al., 2024), compared to -585 nT of the Hydro-Quebec storm that caused a major power outage across Quebec in 1989 (Boteler et al., 1989). The interplanetary shock arrived at ~ 17 UT on May 10, 2024, marking the initial phase of the storm. The strongest current sheet in the CME solar wind is embedded in a high density region (peaking above 100 cm^{-3}) corresponding to the reversal of the interplanetary magnetic field (IMF) with dominant B_y reversing from approximately -60 to 70 nT (Fig. 1) during the main phase of the storm. The impact of the IMF reversal and density pulse causes extreme variations (4300 nT) in geomagnetic fields (Ohtani et al., 2025). The IMF reversal at 22:30 UT on May 10, Fig. 1 spans more than $100 R_E$ transverse to the Sun-Earth line, since both Wind and ACE observe similar IMF profiles at L1. This study focuses on the soft X-Ray perspective of the dayside magnetopause and cusp dynamics around the impact time of this large-scale dense CME current sheet. Soft X-Ray reconstruction for other intervals of the May 2024 storm has been performed to address the magnetopause position variations under changing IMF (Gong et al., 2025).

Using soft X-rays to image regions of the global magnetosphere is the goal of several missions, including the recent Lunar Environment heliospheric X-ray Imager (LEXI) (B. Walsh et al., 2024), the upcoming Solar wind-Magnetosphere-Ionosphere Link Explorer (SMILE) (Wang et al., 2025), and the mission concept Solar-Terrestrial Observer for the Response of the Magnetosphere (STORM) (Sibeck et al., 2023). The reconstruction of the expected X-ray images from simulation data has been demonstrated in various works (Kuntz et al., 2015; Sun et al., 2015; B. M. Walsh et al., 2016; Sun et al., 2019; Connor et al., 2021; Matsumoto & Miyoshi, 2022; Ng et al., 2023; Grandin et al., 2024), and has shown the plausibility of observing magnetopause motion, flux-transfer events, magnetosheath mirror-mode structures, and the bombardment of foreshock turbulence.

Following the modeling process described in detail in (Ng et al., 2023), we reconstruct X-ray emission around the impact time of the dense CME current sheet using a soft X-Ray model and output from a global geospace simulation driven by spacecraft mea-

surements. Our simulated soft X-Ray imaging provides the first global view of the day-side magnetopause and cusps driven by a dense CME current sheet. In Section 2 we discuss the MHD simulations and the X-ray emission model used to calculate the X-ray intensities. In Section 3 we discuss the images produced and the observable physical phenomena, followed by a discussion of future possibilities and a summary in Section 4.

2 Soft X-ray model and global geospace simulation

In this work we use a previously established soft X-Ray production model (Cravens et al., 2001; Kuntz et al., 2015; Connor et al., 2021) and data from global geospace simulations of the CME event to reconstruct soft X-Ray emission intensity driven by the interaction between solar wind heavy ions and the H in the geocorona.

2.1 Soft X-ray model

The X-ray intensity calculation is (Kuntz et al., 2015; Connor et al., 2021; Cravens et al., 2001; Ng et al., 2023):

$$R_{xray} = \int \frac{\alpha}{4\pi} N_p N_N v_{\text{eff}} ds \left[\text{eV cm}^{-2} \text{s}^{-1} \text{sr}^{-1} \right], \quad (1)$$

where $v_{\text{eff}} = \sqrt{v_b^2 + v_t^2}$ is the effective velocity. v_b is the bulk ion velocity while v_t is the thermal velocity and N_p is the ion density. Due to the nature of the simulation, these are MHD plasma quantities. The integral is line-of-sight and is taken along different angles in the field-of-view of the imager.

The parameter α is a scale factor that determines the soft X-ray production and includes the cross-sections, relative compositions, and transitions for heavy ion states that can give rise to soft X-rays, with $\alpha = 6 \times 10^{-16} \text{ eV cm}^2$ for X-rays in the 100 eV to 1 keV range (Connor et al., 2021; Cravens et al., 2001). N_N is the neutral density and we use a profile

$$N_N = 25 \left(\frac{10R_E}{R} \right)^3 \left[\text{cm}^{-3} \right], \quad (2)$$

where R is the distance from the centre of the Earth and R_E is the Earth radius. The value of 25 cm^{-3} is adopted by the SMILE Modeling Working Group for simulating X-ray images and developing image analysis techniques (Connor et al., 2025). Recent studies on geocoronal and soft X-ray observations (Connor & Carter, 2019; Jung et al., 2025, 2024; Zoennchen et al., 2021) showed that the subsolar hydrogen density at $10 R_E$ is comparable to or higher than 25 cm^{-3} . Thus, 25 cm^{-3} is a good conservative value.

2.2 Global geospace simulation driven by observations

The global geospace simulations are performed using the Multiscale Atmosphere-Geospace Environment (MAGE) model (Lin et al., 2021; Pham et al., 2022). The MAGE configuration used in this study includes the inner magnetosphere model RCM (Toffoletto et al., 2003), ionospheric potential solver REMIX (Merkin & Lyon, 2010), the thermosphere-ionosphere coupling model TIE-GCM (Richmond et al., 1992), and the global MHD model GAMERA (Zhang et al., 2019; Sorathia et al., 2020). The configuration of the model is similar to that used by Sorathia et al. (2023) with the inner boundary at $1.5 R_E$. The GAMERA warped spherical grid is aligned with the Solar Magnetic (SM) X -direction and uses $96 \times 96 \times 128$ cells in the radial, azimuthal and polar directions respectively for simulating this event. The results presented in this work have been interpolated to a uniform Cartesian grid with $0.2R_E$ resolution.

The MAGE simulation presented here is the same as previously used by Ohtani et al. (2025). For the solar wind and IMF conditions, we use a combined upstream MMS

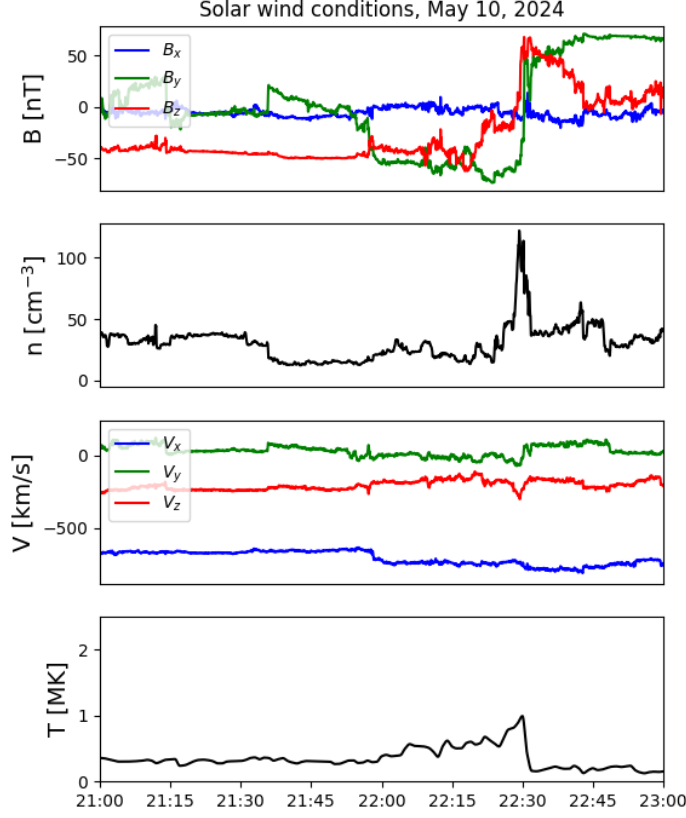


Figure 1. Upstream magnetic field (B), density (n), velocity (V) and temperature (T) used as the simulation input. The data were measured by MMS (B , n , V) and Wind (T), and all data have been time-shifted to the bow shock nose. The reversal of the magnetic field B_y and B_z is associated with a density pulse reaching 120 cm^{-3} and a temperature drop immediately after the density pulse.

(B , n , V) and Wind (T) data set as input (Fig. 1). We focus on the interval that encompasses the density pulse associated with the reversal of the IMF B_y and B_z at approximately 22:30 UT.

3 Results

In this Section, we present the dayside magnetosphere in soft X-Ray with the X-ray intensity in an example 3D volume rendering and using the results of line of sight integration. The X-Ray intensity at each pixel at 22:36 UT is visualized together with a selection of magnetic field lines (Figure 2, top). IMF field lines are drawn in cyan. Red and green field lines connect to the southern and northern cusps respectively while the magenta field lines are closed. The X-ray signal is strongest in the cusps and in the magnetosheath. The sphere placed at $(0, y = 30R_E, 0)$ illustrates a possible position of the imaging spacecraft (taken as the STORM mission) and the yellow line illustrates the line-of-sight along which an integral is taken. The 3D volume rendering represents the in-

tegrand of equation (1), calculated using the output of the global simulation. The signal in the closed field-line region is set to zero assuming that the high-charge state ions cannot enter the dayside closed-field-line region within the time scale of our study (Sibeck et al., 2018). A line-of-sight integral is then performed from the imager location. We use the angular resolution of the X-Ray imager in the STORM mission concept (Sibeck et al., 2023; Murphy et al., 2024), designed to study the global solar wind-magnetosphere interaction.

The reconstructed X-ray images of the dayside magnetopause and cusps reveal the 3D magnetosphere reconfiguration around the time of the dense CME current sheet arrival. We follow the evolution using spacecraft placed at $(0, y = 30R_E, 0)$ and $(0, 0, z = 30R_E)$ as shown in Fig. 2. These are planned locations of the STORM mission, which is intended to have a $30R_E$ orbit perpendicular to the ecliptic plane. The angular resolution of the presented data is $0.25^\circ \times 0.25^\circ$, the intended resolution of the STORM X-Ray imager. Here θ_1 and θ_2 define the viewing angles, with θ_1 corresponding to the looking direction towards different X , and θ_2 the north-south (the “ $y = 30R_E$ ” row) or dawn-dusk (the “ $z = 30R_E$ ” row) directions.

The arrival of the density pulse can be seen from images at 22:31 to 22:34 UT, with multiple local maxima in the intensity at positive θ_1 corresponding to the density peaks modulated by the $1/R^3$ structure of the neutrals. The innermost intensity peak corresponds to the magnetopause position, where the line of sight viewed from $y = 30R_E$ is tangent to the subsolar magnetopause surface. There is an approximate fourfold increase of the peak intensity from 22:31 to 22:34 UT along $\theta_2 = 0$ in the magnetosheath. The magnetopause moves toward Earth from 22:20 to 22:34 UT with the closest distance at $\sim 4R_E$ (Figure 3) as the dense current sheet (IMF reversal and density pulse) arrives, and the magnetopause expands away from Earth from 22:34 to 22:50 UT as the dense current sheet passes the magnetopause.

The two cusps manifest themselves as two emission ridges in X-Ray with the northern cusp substantially brighter than the southern cusp (Figure 2, top row of thumb-nail panels). This asymmetry is due to the sunward dipole tilt as well as the southward component of the solar wind flow leading to higher solar wind flux into the northern cusp. The two ridges are nearly parallel to each other and the sun-earth line until $\sim 22:33$ UT, approximately three minutes after the IMF reversal from southward to northward. Thereafter, the cusp X-Ray emission ridges move poleward, as the magnetopause retreats farther away from Earth. The nearly parallel cusp ridges and the pushed-in magnetopause location indicate that the dayside magnetic flux (closed field lines) is highly eroded. The northward turning of the IMF starts magnetic reconnection poleward of the cusps, and consequently the two cusp ridges move poleward and away from each other. X-Ray imaging provides a global view of the magnetic flux erosion and re-generation process, and the possibility to quantify the variation of the flux content as well as the time scale. For example, the addition of flux to the dayside can be seen through both the displacement of the magnetopause in the positive θ_1 direction as well as the cusp moving poleward. The area corresponding to the closed-field-line-region (bounded by the two cusps and the magnetopause) of the magnetosphere in the reconstructed images is approximately four times larger at 22:50 UT compared to that at 22:34 UT.

As mentioned earlier, the magnetopause position can be identified by finding the peak intensity along θ_1 , or a peak in its second derivative (Connor et al., 2021; Collier & Connor, 2018). The motion of the magnetopause is illustrated in Figure 3. The top-left panel shows the location of the last closed field line along x at $y = 0, z = 0$ in the simulation, and there is abrupt inward displacement of the magnetopause to within 4–5 R_E radial distance at around 22:34 UT, followed by relaxation. This unusually short distance of the magnetopause standing off the CME wind is consistent with observations by THEMIS (constrained to be $< 6R_E$ (Fu et al., 2025)) and Arase (~ 5 – $6R_E$ (Miyoshi et al., 2025)) spacecraft. The bottom left panel shows the magnetopause position inferred

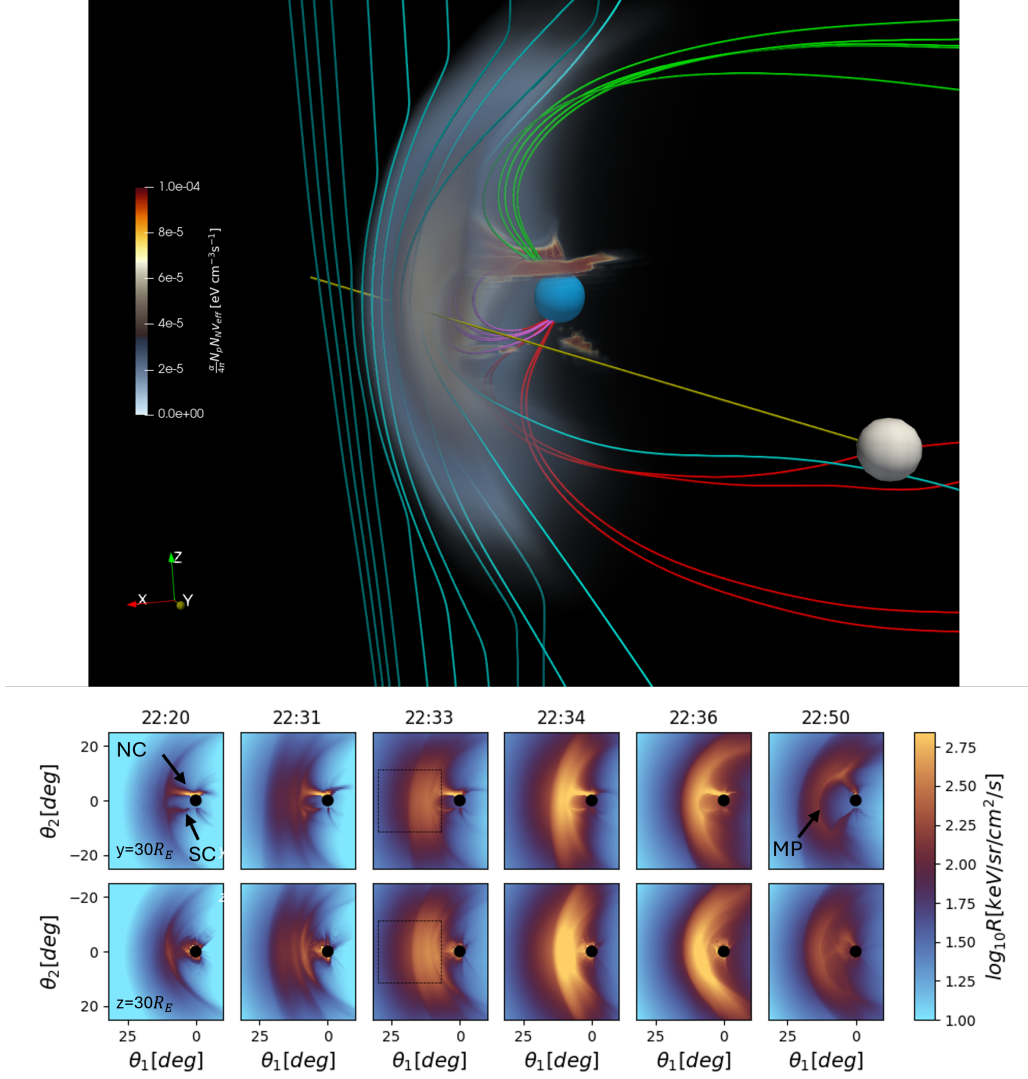


Figure 2. (Top) Volume rendering of the integrand of Equation (1) at 22:36 UT. The white sphere and yellow line show a line-of-sight from a spacecraft positioned at $y = 30R_E$ ($x = z = 0$). IMF field lines are drawn in cyan. Red and green field lines connect to the southern and northern cusps respectively. Magenta field lines are closed. (Bottom) Soft X-ray intensity after line of sight integration observed by an imager at $[0, 30, 0] R_E$ (top row) and at $[0, 0, 30] R_E$ (bottom row). The soft X-ray images are constructed with an angular resolution $0.25^\circ \times 0.25^\circ$. The STORM mission is designed to have an angular resolution 0.17° to 0.25° and a field of view marked by the boxes. Annotations show Northern cusp (NC), Southern cusp (SC) and magnetopause (MP). All vectors are in the SM coordinates.

from the X-ray intensity using either the maximum intensity or the minimum of $d^2 R_{xray}/d\theta_1^2$. Both methods produce general agreement with the result from magnetic topology, even though there is a discrepancy around the arrival time of the density pulse, with the maximum intensity method showing a more sunward magnetopause position. The cause is illustrated in the right panel, which shows the variation of intensity along θ_1 at $\theta_2 = 0$, in which the colours represent time. The arrival of the CME current sheet can be seen in the increase of the X-ray intensity sunward of the magnetopause (larger θ_1), with the maximum intensity observed due to the dense current sheet rather than the magnetopause boundary at certain times. More complex methods exist that extract the magnetopause location in GSE coordinates from soft X-ray emission peak angles and determine the shape of magnetopause (e.g. Collier and Connor (2018); Kim et al. (2023); Cucho-Padin et al. (2024); Gong et al. (2025)).

What would the STORM soft X-Ray imager observe under extreme solar wind conditions such as the May 2024 storm? In Figure 2 we show the expected results using the field of view of the proposed STORM imager, which is $23^\circ \times 23^\circ$ field of view pointed 18.5° sunward of nadir, and is illustrated by the dashed box in Figure 2. STORM will be able to track the magnetopause position over time, as the density pulse pushes the subsolar magnetopause closer and closer to Earth up to $\sim 4R_E$ radial distance. At 22:34 UT, when the magnetopause position reaches $X \sim 4-5R_E$, the subsolar magnetopause is still visible, although it is close to the Earthward edge of the planned field of view of the STORM imager.

The question of whether this X-ray signal can be measured is important. The results thus far are instantaneous, whereas an actual instrument would have finite time integration and be affected by backgrounds. During the arrival of the CME current sheet, the peak intensity in the magnetosheath is over $800 \text{ keV cm}^{-2}\text{s}^{-1}\text{sr}^{-1}$, compared to the diffuse soft X-ray background of $10-30 \text{ keV cm}^{-2}\text{s}^{-1}\text{sr}^{-1}$ (Sibeck et al., 2018). Based on previous work on reconstructions (B. M. Walsh et al., 2016), this unusually high signal from the magnetosheath, because of the high density, would enable high cadence (sub 1 minute) images to be captured.

4 Summary and Discussion

Our simulated soft X-Ray images reveal the global dynamics of the dayside magnetopause and cusps during the May 2024 storm, particularly in response to prolonged strong southward IMF and an unusually dense CME current sheet. Using the MAGE global simulations of the May 10 2024 CME event, we reconstruct the X-Ray images expected to be measured by spacecraft located at $(0, y = 30R_E, 0)$ and $(0, 0, z = 30R_E)$. The combined X-Ray and global simulation results show that (1) the angular position of the magnetopause moves earthward during the arrival of the CME sheet, consistent with spacecraft observations and field-line-tracing simulation results, (2) the cusps in X-Ray emissions move poleward from nearly parallel to each other with a time delay a few minutes after the IMF B_z turns from southward to northward, and the migration to higher and higher latitudes occurs over ~ 10 minutes, and (3) the northern cusp is substantially brighter in X-Ray than the southern cusp.

The global X-Ray view of the magnetopause and cusps complements those from the ionospheric measurements. Based on ionospheric radar measurements from the SuperDARN network (Greenwald et al., 1995), the open-close magnetic field boundary (the low-latitude boundary of the cusp) at $\sim 22:20$ UT is at MLAT $\sim 56^\circ$, and at 22:50 UT, it is further poleward between 62° and 66° . Using a composite model of the cusp location and extent at ionospheric altitudes (constructed from empirical relations of dependences on solar wind conditions and the dipole tilt angle in the literature) (Petrinec et al., 2023) for a southward IMF $B_z = -50 \text{ nT}$ (such as the B_z at 22:20 UT, Figure 1) and a dipole tilt of 18.3° , the equatorward edge of the northern cusp is obtained to be

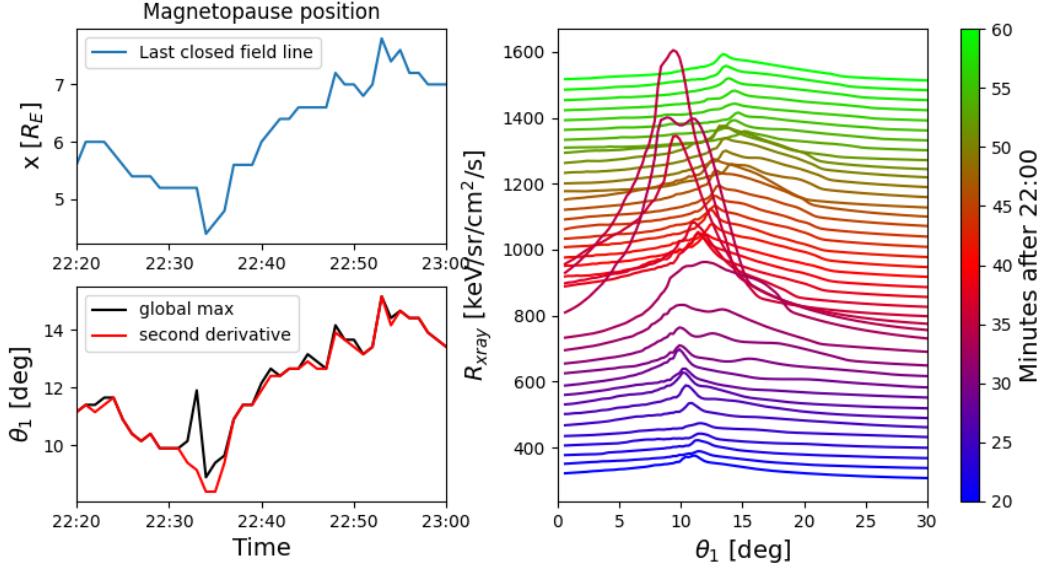


Figure 3. [Left] Magnetopause position determined by magnetic topology (top panel) and extrema in the X-ray intensity and its second derivative (bottom). [Right] X-ray intensity as seen from $y = 30R_E$ along $\theta_2 = 0$ showing the motion of the magnetopause.

58–59°, consistent with the radar observation. When the IMF is northward with $B_z \sim 50$ nT (just after the large IMF B_y rotation, Figure 1) the equatorward edge of the northern cusp is at $\sim 85^\circ$ based on the model. The X-Ray picture shows the large-scale cusp structure in a radial distance range $\sim 1.5R_E$ to $\sim 5R_E$, and its evolution from approximately perpendicular to forming an acute angle with respect to the dipole axis (along positive z in the SM coordinate used in this paper), information not available from the ionospheric measurements or the empirical cusp model.

Soft X-ray imaging can provide simultaneous observations of the impact of solar-wind interactions on different regions of the magnetosphere. As such, it complements in situ measurements of the magnetospheric plasma by providing the global context, such as the locations and structures of the magnetopause, cusps, the bow shock, and magnetosheath. The global X-ray images from future missions will provide large-scale information that is challenging, if not impossible, for even multi-point local measurements to deliver.

Acknowledgments

The work of JN, LJC, and BB was supported by the NASA MMS mission, and the work of KHP and VGM by the NASA DRIVE Science Center for Geospace Storms (CGS) under NASA award 80NSSC22M0163. The MAGE model is developed by CGS. We acknowledge high-performance computing support from NASA High-End-Computing and the Derecho system (doi:10.5065/qx9a-pg09) provided by the NSF National Center for Atmospheric Research (NCAR), sponsored by the National Science Foundation.

Open Research

Data used in this paper are openly available at (Ng et al., 2025).

References

- Boteler, D., Shier, R., Watanabe, T., & Horita, R. (1989). Effects of geomagnetically induced currents in the bc hydro 500 kv system. *IEEE Transactions on Power Delivery*, 4(1), 818–823. doi: 10.1109/61.19275
- Collier, M. R., & Connor, H. K. (2018). Magnetopause surface reconstruction from tangent vector observations. *Journal of Geophysical Research: Space Physics*, 123(12), 10,189–10,199. Retrieved from <https://agupubs.onlinelibrary.wiley.com/doi/abs/10.1029/2018JA025763> doi: <https://doi.org/10.1029/2018JA025763>
- Connor, H. K., & Carter, J. A. (2019). Exospheric neutral hydrogen density at the nominal 10 re subsolar point deduced from xmm-newton x-ray observations. *Journal of Geophysical Research: Space Physics*, 124(3), 1612–1624.
- Connor, H. K., Sibeck, D. G., Collier, M. R., Baliukin, I. I., Branduardi-Raymont, G., Brandt, P. C., ... Zoenchen, J. H. (2021). Soft x-ray and ena imaging of the earth's dayside magnetosphere. *Journal of Geophysical Research: Space Physics*, 126(3), e2020JA028816. Retrieved from <https://agupubs.onlinelibrary.wiley.com/doi/abs/10.1029/2020JA028816> (e2020JA028816) doi: <https://doi.org/10.1029/2020JA028816>
- Connor, H. K., Sun, T., Samsonov, A., Liang, J., Read, A., Li, D., ... others (2025). Smile modeling working group: Modeling and analysis of x-ray and ultraviolet images of solar wind–earth interactions. *Space Science Reviews*, 221(4), 46.
- Cravens, T. E., Robertson, I. P., & Snowden, S. L. (2001). Temporal variations of geocoronal and heliospheric x-ray emission associated with the solar wind interaction with neutrals. *Journal of Geophysical Research: Space Physics*, 106(A11), 24883–24892. Retrieved from <https://agupubs.onlinelibrary.wiley.com/doi/abs/10.1029/2000JA000461> doi: <https://doi.org/10.1029/2000JA000461>
- Cucho-Padin, G., Connor, H., Jung, J., Walsh, B., & G. Sibeck, D. (2024). Finding the magnetopause location using soft x-ray observations and a statistical inverse method. *Earth and Planetary Physics*, 8(1), 184–203. doi: 10.26464/epp2023070
- Fu, W. D., Fu, H. S., Zhang, W. Z., Yu, Y., & Cao, J. B. (2025). Compression of earth's magnetopause down to 5 re during the superstorm on 10 may 2024. *Geophysical Research Letters*, 52(5), e2024GL114040. Retrieved from <https://agupubs.onlinelibrary.wiley.com/doi/abs/10.1029/2024GL114040> (e2024GL114040) doi: <https://doi.org/10.1029/2024GL114040>
- Gong, Y., Sun, T., Tang, B., Guo, Y., Sembay, S., & Wang, C. (2025). Dynamic x-ray imaging of the magnetosheath expected during a super storm. *Frontiers in Astronomy and Space Sciences*, Volume 12 - 2025. Retrieved from <https://www.frontiersin.org/journals/astronomy-and-space-sciences/articles/10.3389/fspas.2025.1563653> doi: 10.3389/fspas.2025.1563653
- Grandin, M., Connor, H. K., Hoilijoki, S., Battarbee, M., Pfau-Kempf, Y., Ganse, U., ... Palmroth, M. (2024). Hybrid-vlasov simulation of soft x-ray emissions at the earth's dayside magnetospheric boundaries. *Earth and Planetary Physics*, 8(1), 70–88. Retrieved from <https://www.eppcgs.org/en/article/doi/10.26464/epp2023052> doi: 10.26464/epp2023052
- Greenwald, R., Baker, K., Dudeney, J., Pinnock, M., Jones, T., Thomas, E., ... others (1995). Darn/superdarn: A global view of the dynamics of high-latitude convection. *Space Science Reviews*, 71(1), 761–796.
- Jung, J., Connor, H., Dimmock, A., Sembay, S., Read, A., & Soucek, J. (2024). Mshpy23: a user-friendly, parameterized model of magnetosheath conditions. *Earth and Planetary Physics*, 8(1).
- Jung, J., Connor, H. K., Carter, J. A., Koutroumpa, D., & Pagani, C. (2025). Exospheric neutral density at the 10 re subsolar point during solar maximum:

- estimates from xmm soft x-ray observations. *Frontiers in Astronomy and Space Sciences*, 12, 1568929.
- Kim, H., Connor, H. K., Jung, J., Walsh, B. M., Sibeck, D., Kuntz, K. D., ... others (2023). Estimating the subsolar magnetopause position from soft x-ray images using a low-pass image filter. *Earth and Planetary Physics*, 8(1).
- Kuntz, K. D., Collado-Vega, Y. M., Collier, M. R., Connor, H. K., Cravens, T. E., Koutroumpa, D., ... Walsh, B. M. (2015, jul). The solar wind charge-exchange production factor for hydrogen. *The Astrophysical Journal*, 808(2), 143. Retrieved from <https://dx.doi.org/10.1088/0004-637X/808/2/143> doi: 10.1088/0004-637X/808/2/143
- Lin, D., Sorathia, K., Wang, W., Merkin, V., Bao, S., Pham, K., ... Anderson, B. (2021). The role of diffuse electron precipitation in the formation of subauroral polarization streams. *Journal of Geophysical Research: Space Physics*, 126(12), e2021JA029792. Retrieved from <https://agupubs.onlinelibrary.wiley.com/doi/abs/10.1029/2021JA029792> (e2021JA029792 2021JA029792) doi: <https://doi.org/10.1029/2021JA029792>
- Matsumoto, Y., & Miyoshi, Y. (2022). Soft x-ray imaging of magnetopause reconnection outflows under low plasma- β solar wind conditions. *Geophysical Research Letters*, 49(19), e2022GL101037. Retrieved from <https://agupubs.onlinelibrary.wiley.com/doi/abs/10.1029/2022GL101037> (e2022GL101037 2022GL101037) doi: <https://doi.org/10.1029/2022GL101037>
- Merkin, V. G., & Lyon, J. G. (2010). Effects of the low-latitude ionospheric boundary condition on the global magnetosphere. *Journal of Geophysical Research: Space Physics*, 115(A10). Retrieved from <https://agupubs.onlinelibrary.wiley.com/doi/abs/10.1029/2010JA015461> doi: <https://doi.org/10.1029/2010JA015461>
- Miyoshi, Y., Shinohara, I., Takashima, T., Asamura, K., Mitani, T. a. H. N., Kasahara, S., ... the ERG Project Team (2025). Arase observations of the radiation belts during the may 2024 geomagnetic storm. *EGU General Assembly*, EGU25-5458. doi: 10.5194/egusphere-egu25-5458
- Murphy, K. R., Shoemaker, M. A., Sibeck, D. G., Schiff, C., Connor, H., Porter, F. S., & Zesta, E. (2024). Target and science visibility of the solar-terrestrial observer for the response of the magnetosphere (storm) global imaging mission concept. *Frontiers in Astronomy and Space Sciences*, Volume 11 - 2024. Retrieved from <https://www.frontiersin.org/journals/astronomy-and-space-sciences/articles/10.3389/fspas.2024.1394655> doi: 10.3389/fspas.2024.1394655
- Ng, J., Burkholder, B., Chen, L.-J., Merkin, V. G., Pham, K. H., Sibeck, D., ... Zou, Y. (2025, September). dataset for: "the may 2024 storm: dayside magnetopause and cusps in simulated soft x-rays". Zenodo. Retrieved from <https://doi.org/10.5281/zenodo.17179578> doi: 10.5281/zenodo.17179578
- Ng, J., Walsh, B. M., Chen, L.-J., & Omelchenko, Y. (2023). Soft x-ray imaging of earth's dayside magnetosheath and cusps using hybrid simulations. *Geophysical Research Letters*, 50(10), e2023GL103347. Retrieved from <https://agupubs.onlinelibrary.wiley.com/doi/abs/10.1029/2023GL103347> (e2023GL103347 2023GL103347) doi: <https://doi.org/10.1029/2023GL103347>
- Ohtani, S., Zou, Y., Merkin, V. G., Wiltberger, M., Pham, K. H., Raptis, S., ... Gjerloev, J. W. (2025). Ground magnetic response to an extraordinary imf by flip during the may 2024 storm: Travel time from the magnetosheath to day-side high latitudes. *Journal of Geophysical Research: Space Physics*, 130(5), e2024JA033691. Retrieved from <https://agupubs.onlinelibrary.wiley.com/doi/abs/10.1029/2024JA033691> (e2024JA033691 2024JA033691) doi: <https://doi.org/10.1029/2024JA033691>
- Petrinec, S. M., Kletzing, C. A., Bounds, S. R., Fuselier, S. A., Trattner, K. J., & Sawyer, R. P. (2023). Trice-2 rocket observations in the low-altitude

- cusps: Boundaries and comparisons with models. *Journal of Geophysical Research: Space Physics*, 128(3), e2022JA030952. Retrieved from <https://agupubs.onlinelibrary.wiley.com/doi/abs/10.1029/2022JA030952> (e2022JA030952 2022JA030952) doi: <https://doi.org/10.1029/2022JA030952>
- Pham, K. H., Zhang, B., Sorathia, K., Dang, T., Wang, W., Merkin, V., ... Lyon, J. (2022). Thermospheric density perturbations produced by traveling atmospheric disturbances during august 2005 storm. *Journal of Geophysical Research: Space Physics*, 127(2), e2021JA030071. Retrieved from <https://agupubs.onlinelibrary.wiley.com/doi/abs/10.1029/2021JA030071> (e2021JA030071 2021JA030071) doi: <https://doi.org/10.1029/2021JA030071>
- Richmond, A. D., Ridley, E. C., & Roble, R. G. (1992). A thermosphere/ionosphere general circulation model with coupled electrodynamics. *Geophysical Research Letters*, 19(6), 601-604. Retrieved from <https://agupubs.onlinelibrary.wiley.com/doi/abs/10.1029/92GL00401> doi: <https://doi.org/10.1029/92GL00401>
- Sibeck, D. G., Allen, R., Aryan, H., Bodewits, D., Brandt, P., Branduardi-Raymont, G., ... others (2018). Imaging plasma density structures in the soft x-rays generated by solar wind charge exchange with neutrals. *Space Science Reviews*, 214, 1-124.
- Sibeck, D. G., Murphy, K. R., Porter, F. S., Connor, H. K., Walsh, B. M., Kuntz, K. D., ... Cramer, W. D. (2023). Quantifying the global solar wind-magnetosphere interaction with the solar-terrestrial observer for the response of the magnetosphere (storm) mission concept. *Frontiers in Astronomy and Space Sciences, Volume 10 - 2023*. Retrieved from <https://www.frontiersin.org/journals/astronomy-and-space-sciences/articles/10.3389/fspas.2023.1138616> doi: 10.3389/fspas.2023.1138616
- Sorathia, K. A., Merkin, V. G., Panov, E. V., Zhang, B., Lyon, J. G., Garrettson, J., ... Wiltberger, M. (2020). Ballooning-interchange instability in the near-earth plasma sheet and auroral beads: Global magnetospheric modeling at the limit of the mhd approximation. *Geophysical Research Letters*, 47(14), e2020GL088227. Retrieved from <https://agupubs.onlinelibrary.wiley.com/doi/abs/10.1029/2020GL088227> (e2020GL088227 10.1029/2020GL088227) doi: <https://doi.org/10.1029/2020GL088227>
- Sorathia, K. A., Michael, A., Merkin, V. G., Ohtani, S., Keesee, A. M., Sciola, A., ... Pulkkinen, A. (2023). Multiscale magnetosphere-ionosphere coupling during stormtime: A case study of the dawnside current wedge. *Journal of Geophysical Research: Space Physics*, 128(11), e2023JA031594. Retrieved from <https://agupubs.onlinelibrary.wiley.com/doi/abs/10.1029/2023JA031594> (e2023JA031594 2023JA031594) doi: <https://doi.org/10.1029/2023JA031594>
- Sun, T. R., Wang, C., Sembay, S. F., Lopez, R. E., Escoubet, C. P., Branduardi-Raymont, G., ... Guo, Y. H. (2019). Soft x-ray imaging of the magnetosheath and cusps under different solar wind conditions: Mhd simulations. *Journal of Geophysical Research: Space Physics*, 124(4), 2435-2450. Retrieved from <https://agupubs.onlinelibrary.wiley.com/doi/abs/10.1029/2018JA026093> doi: <https://doi.org/10.1029/2018JA026093>
- Sun, T. R., Wang, C., Wei, F., & Sembay, S. (2015). X-ray imaging of kink-helmholtz waves at the magnetopause. *Journal of Geophysical Research: Space Physics*, 120(1), 266-275. Retrieved from <https://agupubs.onlinelibrary.wiley.com/doi/abs/10.1002/2014JA020497> doi: <https://doi.org/10.1002/2014JA020497>
- Toffoletto, F., Sazykin, S., Spiro, R., & Wolf, R. (2003). Inner magnetospheric modeling with the rice convection model. *Space science reviews*, 107, 175-196.
- Tulasi Ram, S., Veenadhari, B., Dimri, A. P., Bulusu, J., Bagiya, M., Gurubaran, S.,

- ... Vichare, G. (2024). Super-intense geomagnetic storm on 10–11 may 2024: Possible mechanisms and impacts. *Space Weather*, 22(12), e2024SW004126. Retrieved from <https://agupubs.onlinelibrary.wiley.com/doi/abs/10.1029/2024SW004126> (e2024SW004126 2024SW004126) doi: <https://doi.org/10.1029/2024SW004126>
- Walsh, B., Kuntz, K., Busk, S. e., Cameron, T., Chornay, D., Chuchra, A., ... others (2024). The lunar environment heliophysics x-ray imager (lexi) mission. *Space Science Reviews*, 220(4), 37.
- Walsh, B. M., Collier, M. R., Kuntz, K. D., Porter, F. S., Sibeck, D. G., Snowden, S. L., ... Thomas, N. E. (2016). Wide field-of-view soft x-ray imaging for solar wind-magnetosphere interactions. *Journal of Geophysical Research: Space Physics*, 121(4), 3353–3361. Retrieved from <https://agupubs.onlinelibrary.wiley.com/doi/abs/10.1002/2016JA022348> doi: <https://doi.org/10.1002/2016JA022348>
- Wang, C., Branduardi-Raymont, G., Escoubet, C. P., & Forsyth, C. (2025). Solar wind magnetosphere ionosphere link explorer (smile): science and mission overview. *Space Science Reviews*, 221(1), 9.
- Zhang, B., Sorathia, K. A., Lyon, J. G., Merkin, V. G., Garretson, J. S., & Wiltberger, M. (2019). Gamera: A three-dimensional finite-volume mhd solver for non-orthogonal curvilinear geometries. *The Astrophysical Journal Supplement Series*, 244(1), 20.
- Zoennchen, J. H., Connor, H. K., Jung, J., Nass, U., & Fahr, H. J. (2021). Terrestrial exospheric dayside h-density profile at 3–15 r_e from uvis/hdac and twins lyman- α data combined. *Annales Geophysicae Discussions*, 2021, 1–16.